Analysis of Strength Characteristics and Energy Dissipation of Improved-Subgrade Soil of High-Speed Railway above Mined-Out Areas

Shuren WANG*, Kunpeng SHI, Yubo CHEN, Jiyun ZAHNG, Chunliu LI

Abstract: To reveal the effect of sand content on the mechanical performance and energy dissipation of cement improved subgrade soil, using universal testing machine and SHPB test device, unconfined compressive strength (UCS) and impact compression strength under different impact load (0.2, 0.3, 0.4, and 0.5 MPa) were carried out for the cement improved subgrade soil with different sand content (0%, 5%, 10%, 15%, and 20%). Results show that the dynamic and static stress-strain curves of the cement improved soil have similar variation trend. With the increase of the sand content, the UCS and impact compressive strength of the cement improved soil both increase first, then decrease later, showing the form of a quadratic function. The strength growth rate and the dynamic increase factor (*DIF*) reach the maximum values when the sand content is 10%, which is 64.7% and 18.6% larger than that of ordinary improved subgrade soil, respectively. In addition, when the sand content increases from 0% to 20%, the specific dissipation energy increases first, and decreases later. Mixing 10% natural sand is the optimal proportion to obtain better energy dissipation capacity of the sand-cement-improved soil.

Keywords: dynamic test; energy dissipation; high-speed railway; mined-out area; subgrade soil

1 INTRODUCTION

In recent decades, as an efficient, safety and environment-friendly means of transportation, the high-speed railway has received extensive attention in many countries. However, with the rapid development of the high-speed railway, the construction density of the high-speed railway network is increasing, and the available land resources are decreasing. Some high-speed railway lines have to cross the soft soil areas, mined-out areas and other defective geological areas [1-3].

For the special foundation engineering of the mined-out areas, during the operation of the high-speed railway, the disturbance of train dynamic loading on the foundation should be reduced to ensure the energy generated by the vibration load being transmitted to the foundation as little as possible. So, it is necessary to improve the energy absorption capacity of the subgrade fillers on the basis of meeting the anti-deformation capacity under dynamic loading, so as to reduce the impact of the train dynamic loading on the foundation of the mined-out areas.

Compared with buildings, the high-speed railway involves a large scope, has a long service life, and has higher requirements on the stability and deformation of the roadbed [4-6]. At present, the treatment method for the foundation of the mined-out areas under the railway is relatively single and simple, and the grouting work is usually designed and arranged based on the engineering experience. The grouting scope is wide, and the blindness is large, which sometimes causes great waste and also carries a certain degree of risk. So, the research on the treatment methods should not be limited to the grouting method, and it has high research value by changing the subgrade and pavement structure, improving the mechanical performances of the subgrade soil filling.

2 STATE OF THE ART

At present, a great diversity of additives such as natural sand, fiber and cement have been used to improve the defective roadbed fillers to meet the needs of engineering practice [7, 8]. Elahi et al. mixed cement and fly ash into

the soil in different proportions to produce compressed-stabilized soil blocks to replace traditional building materials, and they evaluated the compressive strength, splitting tensile strength and other mechanical properties of the materials under experimental conditions such as dry-wetting cycle and weathering [9]. Renjith et al. studied the addition of 1% 1:500 diluent which could significantly improve the stability of modified soil; and the addition of 2% lime could also improve its bearing capacity [10]. In addition, the combination of fly ash and slag powder as binder could alleviate the expansion potential of expansive soil to a certain extent, and provide new possibilities for improving unconfined compression strength. Dayioglu et al. used expansive clay in South Dakota as material, mixing with different grades of fly ash and lime. They conducted the expansion pressure and the UCS of specimens with different curing ages (0, 7, 28 d), and found that fly ash and lime could significantly improve the UCS of the expansive soil [11].

Due to the stricter requirements for settlement of the subgrade, in order to ensure the dynamic stability of the train under vibration load, the dynamic response of ballast less track subgrade should be fully considered. Long-term dynamic loading and dry-wet cycles are important factors that affect the strength characteristics and long-term stability of the subgrade fillers [12, 13]. Zhong et al. studied the dynamic residual strength and dynamic strength evolution characteristics of the improved loess with different fly ash content after drying and wetting cycle, and they proposed the optimal proportion of 25%-30% fly ash in improved loess according to the quantitative influence of residual deformation and dynamic strength [14]. Zhang et al. discussed the internal relationship between cement content and mechanical properties of loess. In addition, they evaluated its dynamic stability, and recommended that the cement content should be controlled at about 5% for comprehensive consideration [15]. The subgrade settlement standard is generally designed according to the static and cyclic dynamic loading, but the impact on the subgrade is more serious, such as the braking of heavy-duty vehicles, the track irregularity of high-speed trains and impact loads of aircraft taking off and landing on airport

runways [16]. Most researches focused on the dynamic response of the subgrade under vibration load, while the mechanical characteristics of the subgrade fillers under dynamic load are rarely studied.

In terms of the mechanical characteristics of the subgrade improved soil with different admixtures, some scholars mostly focus on dynamic compressive strength and long-term dynamic stability, but do not conduct in-depth research on the failure mode and energy dissipation characteristics of the subgrade improved soil under different impact pressure. Wu et al. carried out the dynamic compression experiment of the cement silty clay with sand by using the split SHPB device. Compared with ordinary cement silty clay, the yield stage of its stress-strain curve was less obvious [17, 18]. Wang et al. established a two-factor equation among the dynamic strength increase factor, strain rate and confining pressure through the SHPB test [19, 20]. Sedighi et al. carried out a series of numerical calculations on the soil improvement technology of shotcrete column through the finite element method, and they evaluated the seismic performance and brittle failure characteristics of shotcrete column under seismic load [21]. Quiroga et al. analyzed the influence of temperature on the failure degree and energy dissipation of sandstone during the failure process, and found that temperature had a significant influence on the energy dissipation [22].

In the past, the subgrade treatment of railway was mostly analyzed from the perspective of whether the anti-deformation ability of the improved subgrade soil itself reached the deformation control standard, that is, only from the perspective of the static mechanical properties of the improved soil. The mechanical performances and energy dissipation of the cement improved subgrade under long-term dynamic load and transient impact load were considered little. To reveal the dynamic and static mechanical performances and energy dissipation relationship of the cement-improved-subgrade soil with different sand content [23, 24], the subgrade soil in the construction site of Taijiao line was selected as the research object, and the UCS and uniaxial impact compression tests of the cement improved-subgrade soil with sand content of 0%, 5%, 10%, 15%, and 20% are carried out, respectively. The dynamic and static compressive strength and energy dissipation characteristics of the improved-subgrade soil were preliminarily discussed.

The remainder of this study is organized as follows. In Section 3, the materials and samples are described, and the test equipment and scheme are stated. In Section 4, the strength and energy dissipation characteristics of the improved-subgrade soil are analyzed and discussed. Finally, some conclusions are given in Section 5.

3 METHODOLOGY
3.1 Materials and Samples Preparation

In practical engineering, cement slurry was usually selected as the condensed material for the improved subgrade soil, and the cement content is 3%, 5% and 7%. Previous studies have found that when the cement content increases from 3% to 7%, the cumulative plastic deformation of the improved roadbed soil decreases from 0.80 mm to 0.30 mm, which is a reduction of 62.3%, while the cost has increased by 133.3%. On the basis of satisfying

the subgrade deformation control standard, in order to ensure the construction quality and the principle of saving cost, it is necessary to improve the type and dosage of aggregates of subgrade fillers to ensure the stability of the foundation of the mined-out areas. Considering the defects of the foundation and the high safety grade of the high-speed railway subgrade, the relatively low-cost natural sand as the aggregate was selected to improve the resist deformation ability of the high-speed railway subgrade soil. The natural sand was mixed into the improved-subgrade filler with 5% cement in different dosages, and the effect of sand on the energy consumption of the improved-subgrade-soil was studied.

The soil samples needed for the test were taken from the construction site of Taijiao high-speed railway in Jiaozuo, China. According to the standard of geotechnical test, the soil sampling method was adopted in situ. The density of undisturbed subgrade soil was 1780 kg/m^3 and the optimal moisture content was 11.8%. The cement mixed into the soil sample was portland cement (P.O 42.5). The best moisture content of the remold subgrade soil with cement content of 5% was 15.4% by compaction test. The sand was naturally fine river sand below 5 mm obtained from Henan Province as shown in Fig. 1.
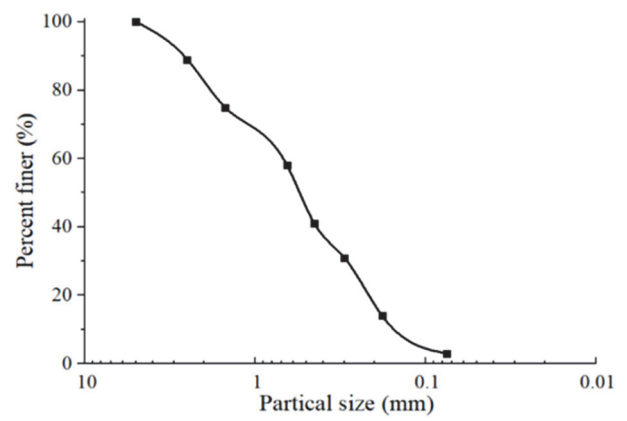
Figure 1 Partical size of sand

The remold subgrade soils were prepared, and the cement-improved-subgrade soils with sand content of 0%, 5%, 10%, 15% and 20% were prepared to fabricate the UCS and SHPB impact test specimens, as shown in Fig. 2.

(a) SHPB specimens   (b) Compressive strength specimens
Figure 2 Specimens of improved subgrade soil

The diameter of UCS sample was 50 mm with the height 100 mm. During preparation, five layers were rammed and each layer was shaved. The diameter of SHPB sample was 50 mm with the height 25 mm. During preparation, three layers were tamped and each layer was shaved. Finally, the samples were put into a sealed bag and moved to a standard curing room for 28 d.

3.2 Test Equipment and Scheme

As shown in Fig. 3, the θ50 mm separated variable section SHPB test system and universal testing machine in Henan Polytechnic University were adopted in this study. The maximum test force of universal testing machine WDW-50 was 50 kN, the test level was 0.6. The SHPB impact device was composed of gas pressure system, elastic pressure bar system, buffer damping device and data acquisition and processing system. The nitrogen was used in the test and different impact pressures were adjusted by the air pressure controller.

(a) Universal testing machine   (b) SHPB impact equipment
Figure 3 Testing equipment

To prepare the SHPB impact test, the sample needed to be placed at the designated position, and the axial stress of 0.1 MPa was applied by the axial loading device to ensure the close contact between the specimen and the testing apparatus without falling off. The schematic diagram of impact devices is shown in Fig. 4.

Figure 4 Schematic diagram of impact devices
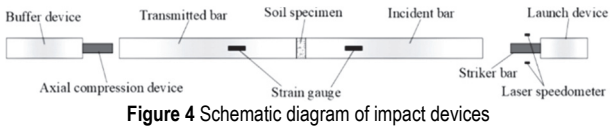
To obtain the dynamic and static stress-strain curves and energy dissipation characteristics of the cement improved soil with different sand content, the UCS of the specimens was tested by the WDW-50 testing device, and the microstructure of the broken soil samples was observed and analyzed by SEM. The dynamic impact test of the cement improved soil with 0%, 5%, 10%, 15% and 20% sand was carried out by using SHPB test equipment, and the impact gas pressure in the impact compression test was 0.2 , 0.3, 0.4 , and 0.5 MPa, respectively.

4 RESULTS ANALYSIS AND DISCUSSION
4.1 Static Strength Characteristics of Samples

To research the static strength characteristics of the cement improved subgrade soil, the UCS experiment was carried out with different sand contents. The UCS of the cement improved soil sample with sand is shown in Fig. 5. The variation trend of stress-strain curve of the cement improved soil with different sand content is basically the same. In the initial of the USC test, the stress-strain curve basically satisfies a simple linear correlation. With the increase of stress, the primary cracks in the cement

improved soil specimen gradually develop and expand, accompanied by the formation of new micro cracks. The slope of the curve decreases with the increase of stress, that is, it enters the plastic yield stage. It can be seen from Fig. 6, when the peak stress of the cement improved soil is reached, the specimen appears "Y" or "1" type splitting failure, and the stress-strain curve shows a precipitous decline of cliff type, and finally the specimen was split or shear failure. Fig. 5b shows that the UCS of the cement improved soil with sand. The USC of the cement improved soil increases sharply with the increase of the sand content, when the optimal sand content is 10%, it reaches the peak, dropping slowly later. The fitting results meet the quadratic function relationship:

$$\sigma_b = 5.51 + 0.51S - 0.02S^2 \qquad (1)$$

where, σ_b is the stress, S is the sand content.

(a) Stress-strain curve

(b) Strength variation
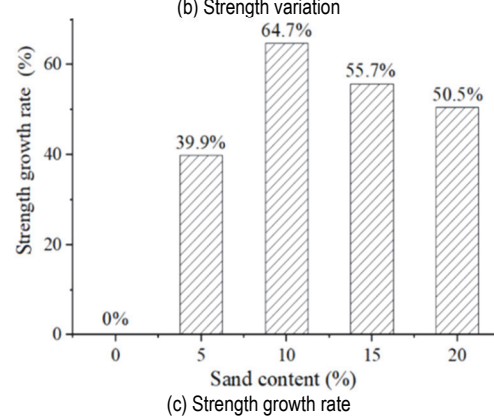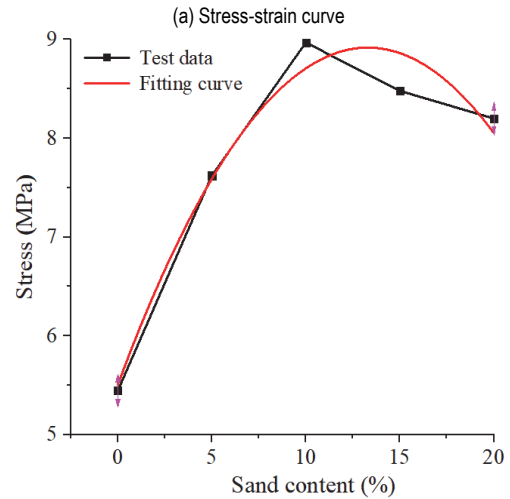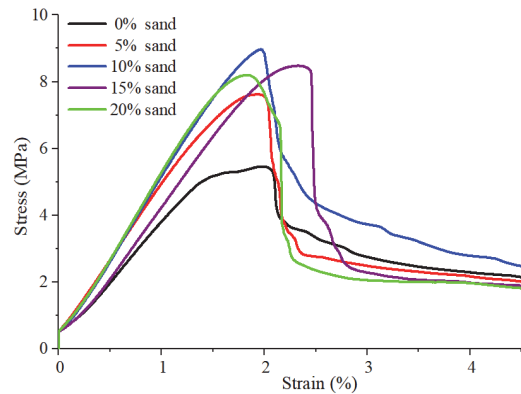
(c) Strength growth rate
Figure 5 UCS of improved-subgrade soil with different sand content

Fig. 5c shows that mixing sand significantly improves the UCS of the improved-subgrade soil. When the sand content is less than 20%, the UCS of the improved soil with sand content increases by more than 40% compared with that without sand. The strength growth rates of UCS of the cement improved soil with 5%, 10%, 15%, and 20% sand content are 39.9%, 64.7%, 55.7%, and 50.5%, respectively. In addition, when the sand content $S = 10\%$, the strength growth rate of the improved soil is the largest.

Figure 6 Failure mode of unconfined compressive strength

To more intuitively analyze the improvement effect of sand on UCS of the improved soil, the strength growth rate is proposed to measure the effect of strength improvement, and the strength growth rate ξ can be calculated by Eq. (2):

$$\xi = \frac{\sigma_s - \sigma_0}{\sigma_0} \qquad (2)$$

where, σ_s is the UCS of the improved soil with sand. σ_0 is the UCS of the improved soil without sand.

4.2 Effect of Sand Content on Microstructure of Improved-Subgrade Soil

The mixing sand has a good improvement effect on improving the UCS of the improved-subgrade soil. To reflect the internal structure changes of soil samples before and after improvement more intuitively, the internal mechanism of improving soil strength with different sand content was clarified. Three kinds of improved soil samples with sand content of 0%, 10% and 20% were selected to analyze the difference of their micro-structures. The micro-structure of the improved soil with different sand content is magnified by 500 times, as shown in Fig. 7.

It can be seen from Fig. 7, the connection interface between soil and cement in the cement improved soil without sand is weak, and there are micro pores among soil particles, so the integrity is relatively poor. With the incorporation of natural sand, sand particles, soil and cement hydration products form a whole, and the space between soil particles is filled with fine sand particles, which plays a supporting role of aggregate to a certain extent. With the addition of sand, a stable structure of sand-soil-cement is formed inside the cement improved soil. Compared with the soil-cement structure without sand, this structure system is more stable and reliable, which is manifested in the increase of strength in terms of macroscopic mechanical properties. However, when the amount of sand is too high, more sand-sand interface will appear, and the stable structure of sand-soil-cement will be replaced. Due to the small friction coefficient the sand-sand joint surface, the overall connectivity of the internal

structure of the soil is reduced. Compared with the sand-soil-cement structure and soil-cement structure, the sand-sand interface is more unstable and prone to damage. Therefore, the macroscopic strength shows a decreasing trend. The stability of the internal structure of the cement improved soil can be optimized when the sand content is 10%.
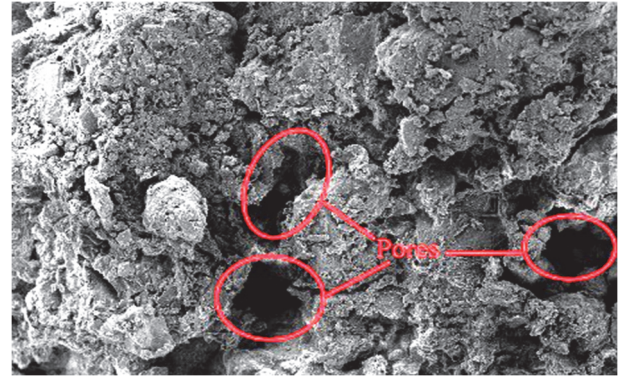
(a) Improved soil without sand

(b) Improved soil with 10% sand
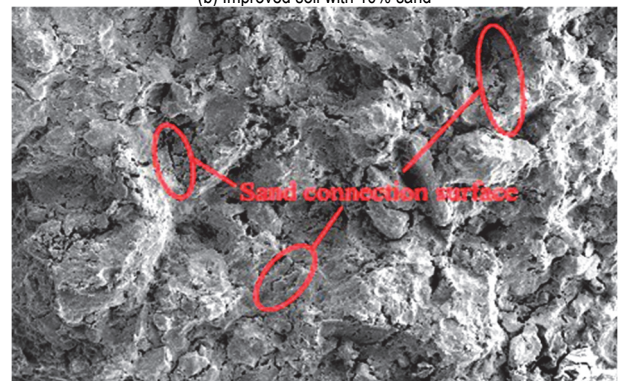
(c) Improved soil with 20% sand
Figure 7 SEM images of improved soil

4.3 Dynamic Peak Stress of Improved-Subgrade Soil

For the strain-rate mechanical tests of the cement improved soil, the stress distribution of the specimen must be maintained uniform before failure [21]. Fig. 8 shows that the overall variation trend of the incident wave and superposition wave is roughly consistent. Therefore, the test results basically meet the stress uniformity through checking.

The strain ε_s, strain rate $\dot{\varepsilon}$, and stress σ_s of sample can be obtained from the experimental data, which are calculated by the following formulas:

$$\begin{cases} \sigma_S = \dfrac{EA_0\varepsilon_T}{A_S} \\[2mm] \dot{\varepsilon} = \dfrac{2C_0(\varepsilon_I - \varepsilon_T)}{L_S} \\[2mm] \varepsilon_S = \dfrac{2C_0}{L_S}\int_0^t (\varepsilon_I - \varepsilon_T)\mathrm{d}t \end{cases} \quad (3)$$

where, ε_I, ε_T is incident and transmitted strain signals measured. A_0 is the lateral section area of the samples, A_s is the initial area of the samples, and L_s is the initial height of the samples. C_0 is the wave speed in the SHPB device.
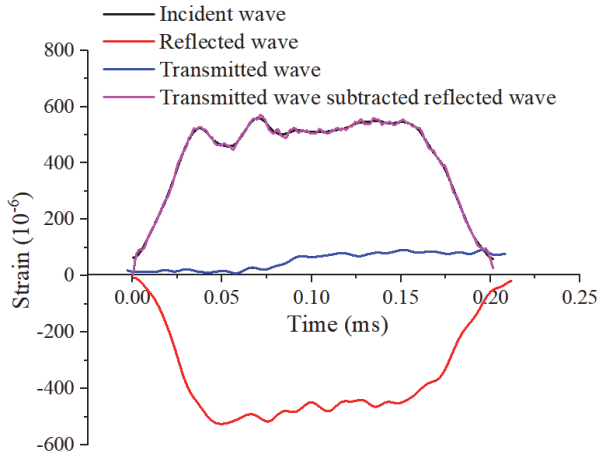
Figure 8 Stress uniformity check (gas pressure 0.4 MPa)

Five groups of the cement improved soil specimen with different sand content were prepared, and the dynamic compression experiment was carried out under four different impact gas pressures by the SHPB devices. The collected wave signals were processed and calculated according to Eq. (3), and the stress-strain curve of the samples with sand under different pressure was obtained, as shown in Fig. 9. The stress-strain curves of specimen are affected by sand content and impact load. Fig. 9 shows that the change trend of the stress-strain curve of the modified soil is basically the same. Moreover, comparing Figs. 8 and 9, the variation trend of dynamic stress-strain curve and static ones of the cement improved soil with sand is similar. The dynamic peak stress (DPS) of the cement improved soil increases first, and decreases rapidly after reaching the maximum value. In addition, under the same impact load, the ultimate strain of the cement improved soil with different sediment concentration is roughly the same, but the DPS of cement modified soil increases first and then decreases. Besides, when the sand content is constant, the DPS of the cement improved soil increases significantly with the impact load increased.

Table 1 Fitting parameters

a	b	c	d	z_0	R^2
4.166	0.868	7.310	−0.037	3.984	0.957

It can be seen from Fig. 10a, the DPS of the cement improved soil is affected by sand content and impact load. As shown in Eq. (4), a two-factor equation for the DPS of the cement improved soil with the changing of the impact load and the sand content is constructed, and the fitting parameters are as shown in Tab. 1:

$$z = z_0 + ax + by + cx^2 + dy^2 \quad (4)$$

where, x is the gas pressure, y is the sand content, z is the DPS.

The fit index of the fitting formula is 0.957, which indicates that the fitting results agree well with the experimental data. In addition, the effect of the impact load on the DPS is more significant than that of the sand content.
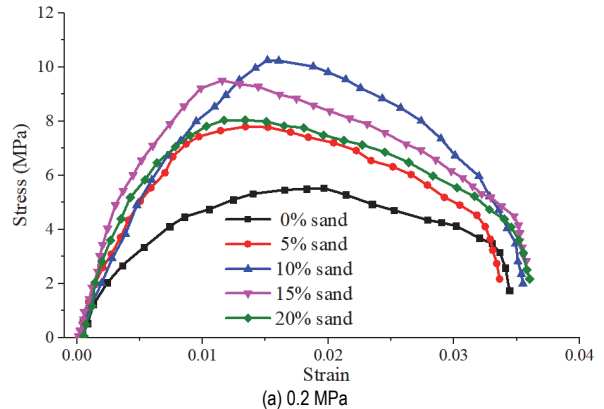
(a) 0.2 MPa
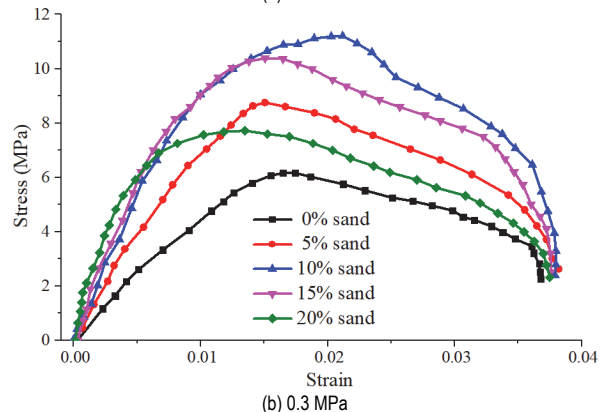
(b) 0.3 MPa
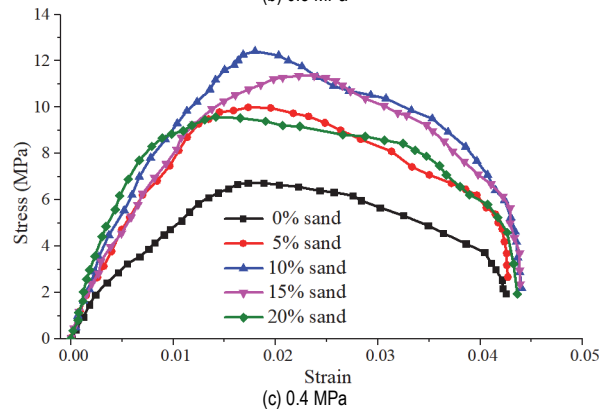
(c) 0.4 MPa
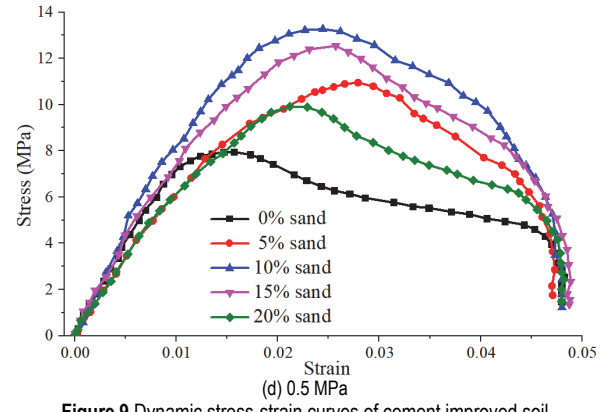
(d) 0.5 MPa

Figure 9 Dynamic stress-strain curves of cement improved soil

The energy reflection coefficient of the soil interface is introduced, and the dynamic increase factor (*DIF*) reflects the changing of the DPS of the cement improved soil under impact load.

$$DIF = \frac{\sigma_d}{f_Q} \qquad (5)$$

where, f_Q is the UCS of the sample. σ_d is the DPS of the sample.

The relationship between the DIF and the impact gas pressure is plotted in Fig. 10b. The impact gas pressure is approximately linear with DIF, which is evidently positively related to the DIF. The amount of sand can improve the DIF of the improved soil to some extent. The increase range of the peak stress of the improved soil can be improved by adding sand under the impact load.

(a) Dynamic compressive strength

(b) Effect of the impact load on DIF
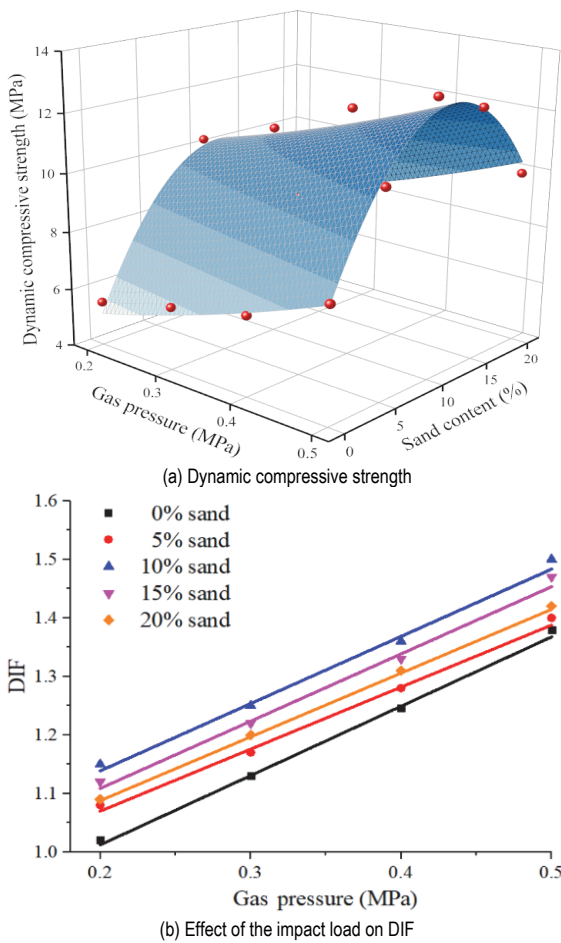
Figure 10 Dynamic mechanical properties of improved-subgrade soil

4.4 Energy Dissipation Characteristics of Samples

To study the energy dissipation characteristics is helpful to reveal the internal mechanism of the cement improved subgrade soil, and the incident, reflected and transmitted energy can be obtained:

$$\begin{cases} W_{\mathrm{I}} = AEC_0 \int \varepsilon_I^2(t)\mathrm{d}t \\ W_{\mathrm{R}} = AEC_0 \int \varepsilon_R^2(t)\mathrm{d}t \\ W_{\mathrm{T}} = AEC_0 \int \varepsilon_{\mathrm{T}}^2(t)dt \end{cases} \qquad (6)$$

where, W_{I}, W_{R} and W_{T} are the incident, reflected and transmitted energy, respectively.

Ignoring the energy loss of the incident and transmission bars and the end face of the sample, the dissipation energy W_{D} is:

$$W_{\mathrm{D}} = W_{\mathrm{I}} - W_{\mathrm{R}} - W_{\mathrm{T}} \qquad (7)$$

By substituting Eqs. (6) into (7), the dissipation energy of the improved-subgrade soil can be expressed as:

$$W_{\mathrm{D}} = AEC_0 \int \varepsilon_{\mathrm{I}}^2(t) - \varepsilon_{\mathrm{R}}^2(t) - \varepsilon_{\mathrm{T}}^2(t)\mathrm{d}t \qquad (8)$$

As seen from Fig. 11, when the impact load is less than 0.3 MPa, the size of the sample fragments after destruction is large. However, as the impact load increases, the number of fragments increases noticeably, the degree of fragmentation of the sample gradually increases, and the geometric size decreases significantly.

| (a) 0.2 MPa pressure | (b) 0.3 MPa pressure |
| (c) 0.4 MPa pressure | (d) 0.5 MPa pressure |

Figure 11 Failure patterns of specimens under impact loads (sand content 10%)

It can be seen from Fig. 12, with the increase of amount of sand content, the debris geometry size decreases, the debris amount increases, and gradually tends to be homogenized. Therefore, with the addition of sand, the impact failure mode of the specimen will be changed to a certain extent.

To reveal the energy dissipation characteristics of the cement improved soil, the specific dissipation energy is introduced to comprehensively characterize the energy dissipation of the cement improved soil crushing. According to the definition, the calculation method is:

$$W_{\mathrm{SDE}} = \frac{W_{\mathrm{D}}}{V} \qquad (9)$$

where, W_{SDE} is the specific dissipation energy, and V is the volume of the specimen.

(a) 0% sand (b) 5% sand

(c) 10% sand (d) 15% sand

(e) 20% sand

Figure 12 Failure patterns of specimens under various sand content (impact load 0.3 MPa)
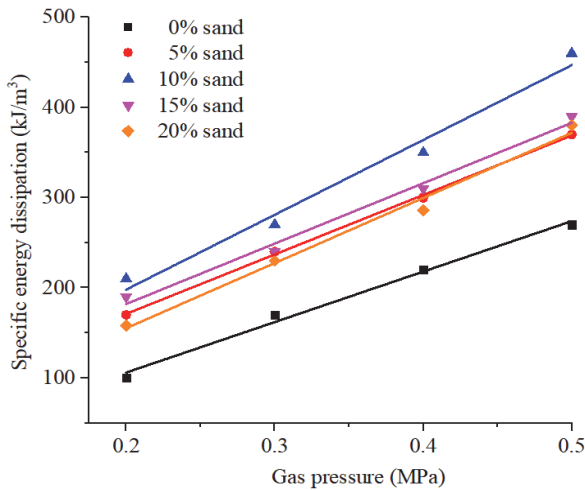
Figure 13 The relationship between specific energy dissipation and impact load

As seen from Fig. 13, the fitting coefficients of the fitting curves are more than 0.95, and the specific dissipation energy of the cement modified soil with sand increases linearly with the increase of impact load. Besides, in the process of impact, the specific energy dissipation of the cement improved soil is also affected by sand content.

Fig. 14 shows that when the impact load is constant, with the increase of sand content S, the specific dissipation energy of the cement improved soil increases first and then decreases. In addition, when $S = 10\%$, the specific

dissipation energy of the specimen reaches the peak value, and when the $S > 10\%$, the specific dissipation energy decreases significantly. When $S < 10\%$, there are a large number of micro pores among the soil particles, which leads to the instability of the internal structure of the cement improved soil. When the optimal proportion reaches $S = 10\%$, the micro pores among the cement improved soil are gradually filled with fine sand particles, and the stable structure of sand-soil-cement is formed inside the specimens, while the natural defects are relatively few.
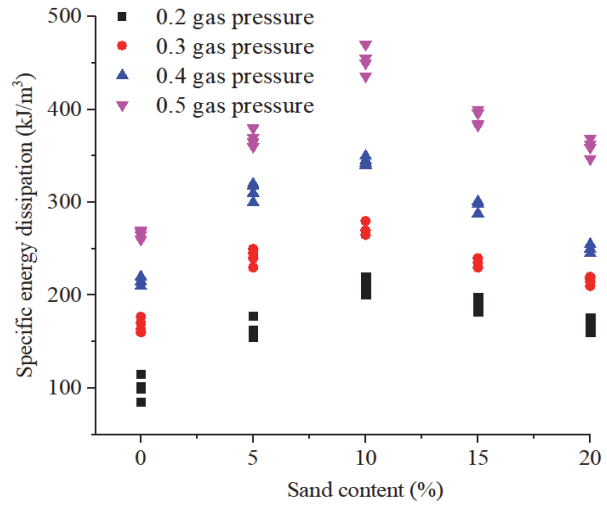
Figure 14 The relationship between specific energy dissipation and sand content

When the cement improved soil is impacted, a lot of micro cracks are formed, while the original cracks are expanding in the improved soil specimens, and the specific dissipation energy of the specimen reaches the maximum at the same time. So, when the sand content increases from 0% to 10%, the specific dissipation energy increases significantly. After adding excessive natural sand ($S = 15\%$ or 20%), there are more sand-sand connected surfaces in the interior of cement improved soil. The sand-sand connected interface is considered to be a primary defect compared to the sand-soil particle interface and sand particle-cement gel interface, which is more vulnerable and prone to slipping failure. Under impact loading, many original micro cracks near the sand-sand interface develop and expand rapidly. Finally, the cement improved soil specimen will break down along the original cracks. The reason is the formation of new fractures that need to consume lots of energy, which is more than the energy needed for the expansion of the primary fractures. Therefore, when $S > 10\%$, the specific dissipation energy begins to decrease.

5 CONCLUSION

To reveal the energy dissipation and mechanical performances of the improved soil mixed with sand for high-speed railway subgrade, on the basis of 5% cement content, five kinds of the cement improved subgrade soil specimens were prepared. The mechanical performances and energy dissipation characteristics of the improved soil mixed with sand under different ratios are analyzed. The main conclusions are as follows:

(1) The incorporation of natural sand fills up the tiny pores between soil particles and forms a stable structure between soil particles and cement hydration products, which significantly enhances the growth of the UCS of the cement-improved-subgrade soil. As the sand content increases from 0 to 20%, the UCS of the improved-subgrade soil increases first, and decreases later. When $S = 10\%$, the strength growth rate reaches the peak of 64.7%.

(2) Sand mixing content of 10% greatly improves the impact resistance of the cement modified soil. The two-factor equation for the DPS of the cement improved soil with the changing of the impact load and the sand content is constructed. In addition, the *DIF* is introduced to comprehensively characterize the growth rate of the DPS of the cement improved soil. When the impact load increases from 0.2 to 0.5 MPa, the *DIF* increases linearly.

(3) The specific dissipation energy of the cement improved soil is affected by the impact pressure and sand content. Under the same sand content, the specific dissipation energy increases with the increase of impact load. When the sand content increases from 0% to 20%, the specific dissipation energy of the cement modified soil first increased and then decreased. Moreover, when S=10%, the dissipation energy of the improved soil reaches the peak value.

In this study, the optimal sand content for energy absorption of the improved foundation soil with sand-mixed cement was obtained. Next step, the optimal content analysis of wastes such as fly ash and steel slag are to be further studied to improve the energy absorption characteristics of the high-speed railway embankment.

Acknowledgements

6 REFERENCES

[1] Li, C. B., Chen, Q. G., Liang, X., & Zhang, S. L. (2014). Model test on pile-plank roadbed of high-speed railway overlying goafs. *Rock and Soil Mechanics*, *35*(11), 3101-3110. https://doi.org/10.16285/j.rsm.2014.11.022

[2] Wang, S. R., Shi, K. P., Zou, Y. F., Zou, Z. S., & Wojciechowski, A. (2021). Coupling deformation between non-uniform settlement of track-structure and subgrade of high-speed railway above the mind-out areas. *Acta Montanistica Slovaca*, *26*(4), 620-633. https://doi.org/10.46544/AMS.v26i4.03

[3] Guo, W. Y., Liu, S. Q., Hu, B. N., Xu, Y. C., & Luo, Y. Q. (2018). Grouting reinforcement of large building foundation over old gob areas: a case study in Huaibei mining area, China. *Advances in Civil Engineering*, *2018*, 8738752. https://doi.org/10.1155/2018/8738752

[4] Solonenko, I. (2019). The equipment for determining the impact of traffic environment on road pavement. *Technical Journal*, *13*(2), 149-153. https://doi.org/10.31803/tg-20190421134423

[5] Bao, W. X., Ma, Z. W., & Wang, H. B. (2020). Integrated treatment technology of storage-mining inclined goaf under expressway. *Advances in Civil Engineering*, *2020*, 8822964. https://doi.org/10.1155/2020/8822964

[6] Wang, S. R., Shi, K. P., Zou, Y. F., Zou, Z. S., Wang, X. C., & Li, C. L. (2021). Size effect analysis of scale test model for high-speed railway foundation under dynamic loading condition. *Tehnicki Vjesnik - Technical Gazette*, *28*(5), 1615-1625. https://doi.org/10.17559/TV-20210208101312

[7] Jamshidi, R. J., Lake, C. B., & Barnes, C. L. (2015). Examining freeze/thaw cycling and its impact on the hydraulic performance of cement-treated silty sand. *Journal of Cold Regions Engineering*, *29*(3), 04014014. https://doi.org/10.1061/(ASCE)CR.1943-5495.0000081

[7] Garcia, S., Garcia, T. T., Espericueta, G. M., & Galvan, I. C. (2022). Nanosilica to Modify the Consistency of High Compressible Lacustrine Clays. *DYNA*, *97*(2), 145-149. https://doi.org/10.6036/10358

[9] Elahi, T. E., Shahriar, A. R., & Islam, M. S. (2021). Engineering characteristics of compressed earth blocks stabilized with cement and fly ash. *Construction and Building Materials*, *277*, 122367. https://doi.org/10.1016/j.conbuildmat.2021.122367

[10] Renjith, R., Robert, D., Setunge, S., Costa, S., & Mohajerani, A. (2021). Optimization of fly ash based soil stabilization using secondary admixtures for sustainable road construction. *Journal of Cleaner Production*, *294*, 126264. https://doi.org/10.1016/j.jclepro.2021.126264

[11] Dayioglu, M., Cetin, B., & Nam, S. (2017). Stabilization of expansive belle fourche shale clay with different chemical additives. *Applied Clay Science*, *146*, 56-69. https://doi.org/10.1016/j.clay.2017.05.033

[12] Luo, P. P., Wang, S. R., Hagan, P., Huang, Q. X., Cao, C., Gamage, K. (2019). Mechanical performances of cement-gypsum composite material containing a weak interlayer with different angles. *DYNA*, *94*(4), 447-454. https://doi.org/10.6036/9191

[13] Shang, Y. H., Xu, L. R., & Cai, Y. (2020). Study on dynamic characteristics of cement-stabilized expansive soil subgrade of heavy-haul railway under immersed environment. *Rock and Soil Mechanics*, *41*(8), 2739-2745. https://doi.org/10.16285/j.rsm.2019.1467

[14] Zhong, X. M., Wang, Q., Liu, D. D., Bai, L., Ma, J. L., Liu, F. Q., Li, N., & Wang, J. (2020). Dynamic strength of fly ash-modified loess subgrade under influences of drying-wetting cycle. *Chinese Journal of Geotechnical Engineering*, *42*(S1), 95-99. https://doi.org/10.11779/CJGE2020S1019

[15] Zhang, P. Y., Ma, X. N., Li, S. Z., & Wang, X. (2019). Long-term dynamic stability evaluation for cement-improved loess subgrade of high speed railway. *Journal of Vibration and Shock*, *38*(11), 80-87. https://doi.org/10.13465/j.cnki.jvs.2019.11.013

[16] Ma, X. N., Zhang, Z., Zhang, P. Y., & Wang, X. (2020). Long-term dynamic stability of improved loess subgrade for high-speed railways. *Proceedings of the Institution of Civil Engineers-Geotechnical Engineering*, *173*(3), 217-227. https://doi.org/10.1680/jgeen.19.00088

[17] Wu, J. R. & Ma, Q. Y. (2015). Uniaxial impact compressive characteristics of permeable asphalt concrete. *Journal of Vibration and Shock*, *34*(4), 195-199. https://doi.org/10.13465/j.cnki.jvs.2015.04.033

[18] Gao, C. H. & Ma, Q. Y. (2018). Analysis of silty clay stabilized by cement mortar based on split hopkinson pressure bar experiment, *Acta Materiae Compositae Sinica*, *35*(6), 1629-1635. https://doi.org/10.13801/j.cnki.fhclxb.20170727.005

[19] Wang, S. R., Wu, X. G., Yang, J. H., Zhao, J. Q., & Kong, F. L. (2020). Mechanical behavior of lightweight concrete structures subjected to 3D coupled static-dynamic loads. *Acta Mechanica*, *231*(11), 4497-4511. https://doi.org/10.1007/s00707-020-02739-y

[20] Wu, X. G., Wang, S. R., Yang, J. H., Zhao, J. Q., & Chang, X. (2022). Damage characteristics and constitutive model of

lightweight shale ceramsite concrete under static-dynamic loading. *Engineering Fracture Mechanics*, *259*, 108137. https://doi.org/10.1016/j.engfracmech.2021.108137

[21] Sedighi, P., Schweiger, H. F., & Wehr, W. J. (2017). Effect of jet-grout columns on the seismic response of layered soil deposits. *International Journal of Geomechanics*, *17*(3), 4016085. https://doi.org/10.1061/(ASCE)GM.1943-5622.0000771

[22] Quiroga, A. J., Thompson, Z. M., Muraleetharan, K. K., Miller, G. A., & Cerato, A. B. (2017). Stress-strain behavior of cement-improved clays: testing and modeling. *ActaGeotechnica*, *12*(5), 1003-1020. https://doi.org/10.1007/s11440-017-0529-1

[23] Wang, Y. F., Wang, S. R., Li, Z., & Jiao, H. J. (2020). Strength characteristics and empirical criterion of dry and saturated sandstone subjected to compression test. *Journal of Engineering Science and Technology Review*, *13*(2), 119-126. https://doi.org/10.25103/jestr.132.16

[24] Zhang, Y. C., Zhang, J. Y., Wang, S. R., & Chen, Y. B. (2021). Controlling vibration speed in tunnel excavation using fine blasting method under complex environmental conditions. *Shock and Vibration*, *202*, 6060485. https://doi.org/10.1155/2021/6060485

Contact information:

Shuren WANG, PhD, Professor
(Corresponding author)
1) International Joint Research Laboratory of Henan Province for Underground Space Development and Disaster Prevention, Henan Polytechnic University
2) State Collaborative Innovation Center of Coal Work Safety and Clean-efficiency Utilization, Henan Polytechnic University,
No. 2001 Century Avenue, Jiaozuo, Henan Province, 454003, China
E-mail: w_sr88@163.com

Kunpeng SHI, PhD, Candidate
School of Civil Engineering, Henan Polytechnic University,
No. 2001 Century Avenue, Jiaozuo, Henan Province, 454003, China
E-mail: 444583054@qq.com

Yubo CHEN, PhD, Candidate
School of Civil Engineering, Henan Polytechnic University,
No. 2001 Century Avenue, Jiaozuo, Henan Province, 454003, China
E-mail: 569079218@qq.com

Jiyun ZHANG, PhD, Candidate
School of Civil Engineering, Henan Polytechnic University,
No. 2001 Century Avenue, Jiaozuo, Henan Province, 454003, China
E-mail: 465743184@qq.com

Chunliu LI, PhD, Associate Professor
School of Urban Construction,
Hebei Normal University of Science and Technology,
No. 360 Hebei West Street, Qingdao, Hebei Province, 066004, China
E-mail: lclcc_010@163.com